Prediction of Dislocation Cores in Aluminum from Density Functional Theory

C. Woodward,[1] D. R. Trinkle,[1,2] L. G. Hector, Jr.,[3] and D. L. Olmsted[4]

[1]*Materials and Manufacturing Directorate, Air Force Research Laboratory, Wright Patterson Air Force Base, Dayton, Ohio 45433-7817, USA*

[2]*Department of Material Science and Engineering, University of Illinois, Urbana-Champaign, Urbana, Illinois 61801, USA*

[3]*General Motors R&D Center, 30500 Mound Road, Warren, Michigan 48090-9055, USA*

[4]*Division of Engineering, Brown University, Providence, Rhode Island 02912, USA*

(Received 21 September 2007; published 31 January 2008)

The strain field of isolated screw and edge dislocation cores in aluminum are calculated using density-functional theory and a flexible boundary condition method. Nye tensor density contours and differential displacement fields are used to accurately bound Shockley partial separation distances. Our results of 5–7.5 Å (screw) and 7.0–9.5 Å (edge) eliminate uncertainties resulting from the wide range of previous results based on Peierls-Nabarro and atomistic methods. Favorable agreement of the predicted cores with limited experimental measurements demonstrates the need for quantum mechanical treatment of dislocation cores.

DOI: 10.1103/PhysRevLett.100.045507 PACS numbers: 61.72.Lk, 61.72.Bb, 61.72.Nn

Plastic deformation in metals is controlled by the creation, motion, and evolution of line defects known as dislocations. Dislocations move at stresses far below that required to irreversibly deform a defect-free crystal [1]. They exhibit multiscale behavior characterized by an atomic-length scale ''core'' at the dislocation center and a long-range strain field that decreases as the inverse of the distance from the core. In fcc metals dislocations can reduce elastic energy by separating into Shockley partial dislocations connected by a stacking fault [1]. For materials with large stacking fault energies (i.e., aluminum) this separation can be quite narrow making experimental investigation of the core structure difficult [2]. Several first-principles methods have been developed that attempt to address the coupling of long-range elastic distortion to the local displacements in the core region [3]. These and atomistic calculations have led to a wide range in the predicted structure of dislocations in Al (cf. Table II).

Accurate modeling of the dislocation core—the local strain field produced by the partials and their separation distance—is key to predictive modeling of plastic behavior in metals. For example, the motion of dislocations in pure Al under stress is governed by geometry-dependent interactions with sound waves (phonon drag) and multiple slip-planes (cross-slip) [1]. Recent models of dynamic strain aging in Al-Mg alloys show that solute binding energies and diffusion activation enthalpies within the dislocation core region control related macroscopic phenomena [12,13]. The most familiar of these is the Portevin-LeChatelier (PLC) effect which is commonly found in commercial Al-Mg alloys [14]. Accurate quantitative inputs to these theories are unavailable due to the approximations inherent in atomistic methods, and the boundary conditions used in previous first-principles approaches. For many alloys correctly describing the atomic scale processes controlling macroscopic phenomena will require quantum mechanical predictions with realistic boundary conditions, this is particularly true for the Al alloys. These alloys have a complex chemistry and flow behavior and play a vital role in a myriad of technical applications.

In this Letter we employ electronic structure calculations based upon density-functional theory (DFT) and a flexible boundary condition method to optimize the strain field of isolated screw and edge dislocations in pure Al. While this methodology has been applied to dislocations in transition metals such as bcc molybdenum and tantalum [15], fcc iridium [16], and ordered alloys [17], the present treatment is the first application to dislocations in a free electron metal. To treat the screw- and edge-character dislocation geometries accurately, simulation cells are designed to minimize electrostatic and strain field interactions with the required surface boundary. Moreover, the long-range dislocation strain field is treated self-consistently using the first-principles lattice Green function boundary condition method (FP-GFBC) [15]. This DFT technique correctly couples the strain field of the dislocation core to the long-range elastic field. When applied to Al the method produces a separation distance for the edge-character dislocation which is in good agreement with the available experimental measurements of these dislocation cores [4].

Computational methods.—The *ab initio* calculations are performed with VASP [18,19], a density-functional code using pseudopotentials and a plane-wave basis. For Al we treat the $3s$ and $3p$ states as valence and employ a plane-wave kinetic-energy cutoff of 192 eV to ensure an accurate treatment of the valence electrons. An initial study was undertaken to determine the optimum pseudopotential representation. Structural parameters are calculated at three levels of increasing accuracy: ultrasoft pseudopotentials [20,21] (USP) in the local density approximation, USP's in the generalized gradient approximation (GGA) of Perdew and Wang [22] and finally projected augmented wave (PAW) method within GGA. The

 © 2008 The American Physical Society

k-point meshes for these initial calculations are $15 \times 15 \times 15$, while the dislocation calculations employ a $1 \times 1 \times 8$ mesh, both use a Methfessel-Paxton smearing of 1 eV. Table I shows the calculated parameters including the shear modulus $[G = (C_{44} + C_{11} - C_{12})/3]$ relating stress and strain along $\langle 110 \rangle$ in the (111) plane. The lattice constant, C_{44} and G significantly improve in going to US-GGA and then PAW-GGA. The wide range of measured stacking fault energies reflects the difficulty of resolving Shockley partial dislocations in Al. The current results are smaller than that calculated previously using norm-conserving pseudopotentials (161 mJ/m^2), and better match augmented plane-wave results (126 mJ/m^2) [27,28]. As a compromise between efficiency and precision the US-GGA potentials are used in the dislocation core calculations.

Calculations of an isolated dislocation requires careful construction of the simulation cell. The cut in the lattice produced by the dislocation (screw or edge) is incompatible with the periodic symmetry imposed by the supercell, so in these calculations a free surface is introduced to contain the dislocation. The vacuum region produces a charge dipole at the surface with slowly decaying Friedel oscillations in the charge density. Our reference calculations show that the atomic forces resulting from the charge dipole extend up to 10 Å from the surface. The relaxation of the edge-character dislocation is calculated in a 58 Å $\times$ 58 Å $\times$ 4.945 Å periodic cell, using 552 atoms in a 24.2 Å radius cylindrical slab surrounded by vacuum. The inner 38 atoms (region I) around the core are relaxed using *ab initio* forces, while the *ab initio* forces of the next 99 atoms (region II) are relaxed using the lattice Green function. The positions of the outer 415 atoms (region III) are updated when minimizing the forces in region II [15]. The relaxation of the screw-character dislocation is calculated in a 68.6 Å $\times$ 68.6 Å $\times$ 2.857 Å periodic cell, using 437 atoms in a 28.3 Å radius cylindrical slab surrounded by vacuum. The inner 63 atoms are in region I, the next 66 atoms in region II, and the remaining 308 atoms in region III. For both dislocations, the *ab initio* forces are relaxed iteratively using conjugate-gradient minimization in region I, followed by lattice Green function updates to minimize the forces in region II, until the atomic forces are less than 5 meV Å^{-1}. Convergence of the strain field with cell size was verified by optimizing larger simulation cells.

A lattice Green function for Al is derived using the calculated elastic constants and the force-constant matrix [29]. The force-constant matrix is calculated using the direct force method in a $3 \times 3 \times 3$ simple cubic supercell (108 atoms), with a $8 \times 8 \times 8$ k-point mesh. The estimated relative error [29] of the calculated lattice Green function due to finite size errors is 1.2%.

Results.—Figure 1 shows the differential displacements (DD) and Nye tensor distribution for the screw and edge components of the $a/2\langle 110 \rangle$ screw-character dislocation including measurements of partial separation. Differential displacements show the relative displacement from a perfect lattice of two nearest neighbor atoms projected in the screw or edge direction by a vector of the corresponding length between the two atoms. The partial dislocations are identified by a triad of atoms whose three vectors have a net chirality (either clockwise or counterclockwise). The Nye tensor distribution uses the atomic displacements of an atom relative to each nearest neighbor to produce a continuous distribution of Burgers vector components; the individual values are projected onto the plane normal to the dislocation line and smoothly interpolated [30]. In this case the partial dislocations are identified by local extrema in the Nye tensor distribution. The width of the Nye tensor distribution shows the partial dislocations spread over several lattice positions, which overlap for the screw com-

TABLE I. Calculated and measured lattice constant, elastic constants (Mbar), and stacking fault energy (mJ/m^2) for fcc aluminum [23–26]. The VASP calculated values are based on different levels of approximation of the pseudopotentials and the local density approximation as described in the text.

Method	a [Å]	C_{11}	C_{12}	C_{44}	G	γ
US-LDA	3.9780	1.218	0.634	0.373	0.319	134
US-GGA	4.0413	1.085	0.568	0.305	0.274	124
PAW-GGA	4.0488	1.0593	0.5708	0.3078	0.264	122
Experiment	4.049	1.130	0.666	0.278	0.247	120-200

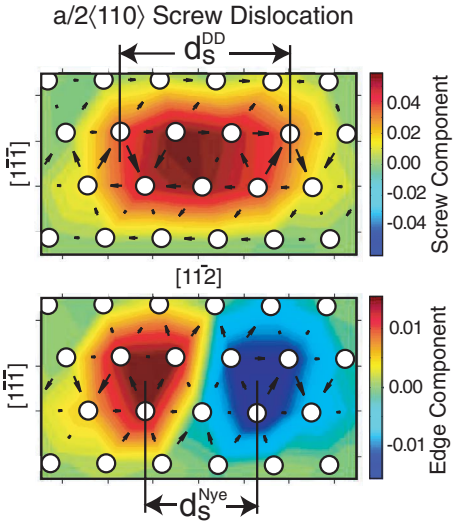

FIG. 1 (color). Atomic core structure (screw and edge components) of the two partials of the $a/2[110]$ screw-character dislocation. The atomic positions (circles) are superimposed on the differential displacements (arrows) and the Nye tensor distribution (color map); see text for details. Using the screw components, the triad of arrows with a net chirality identifies the position of the partials whose separation is d_s^{DD}. From the edge components, the centers of the partials are identified as the extrema in the Nye tensor distribution whose separation is d_s^{Nye}. Using these two measurements the partial core separation is shown to be in the range of 5.0–7.5 Å.

ponent. The DD plot of the screw component gives clear indications of the partial dislocations, as do the extrema in the Nye tensor distribution of the edge components. Using these two approximations the partial core separation is shown to range from $d_s^{\mathrm{DD}} = 7.5$ Å to $d_s^{\mathrm{Nye}} = 5.0$ Å. Comparing the screw and edge components we see that separation distances predicted by each method are self-consistent; however, the Nye tensor gives slightly narrower separation distance. The range of values from the same geometry illustrates the difficulties of defining the center of the partial dislocations to a resolution better than the lattice spacing.

Figure 2 shows the edge and screw components of the edge-character dislocation which has a broader partial separation compared with the screw-character dislocation (Fig. 1). The separation of partials is computed in an identical fashion as for the screw-character dislocation and in this case the DD predicts $d_e^{\mathrm{DD}} = 9.5$ Å and the Nye tensor distribution predicts $d_e^{\mathrm{Nye}} = 7.0$ Å. The narrower width of each partial, along with the smaller lattice spacing in the separation direction increases the accuracy of the separation prediction compared with the screw-character dislocation. However, as with the screw dislocation the Nye tensor produces consistently smaller partial splitting for the edge dislocation as compared to the differential displacement method. Accurate prediction of the dislocation geometry is a crucial first step to understanding the effects of stress, temperature, and solutes on plasticity in Al.

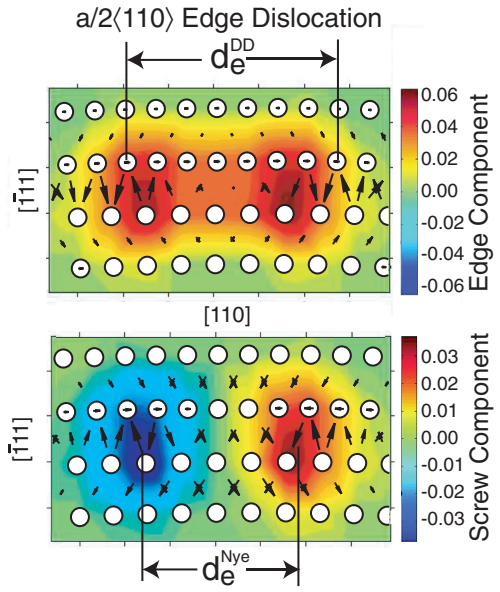

FIG. 2 (color). Atomic core structure (edge and screw components) of the two partials of the $a/2[110]$ edge-character dislocation. As in Fig. 1 the atomic positions (circles) are superimposed on the differential displacements (arrows) and the Nye tensor distribution (color map). Using the edge components, the triad of arrows with a net chirality identifies the position of the partials whose separation is d_e^{DD}. From the screw components, the center of the partials is identified as the extrema in the Nye tensor distribution whose separation is d_e^{Nye}. Using these two measurements the partial core separation is shown to be in the range of 7.0–9.5 Å.

Table II reviews observed and calculated separation distances for the Al screw- and edge-character partial dislocations, revealing a broad range of results [4–11]. Our result for the partial separation distance in the edge-character dislocation is in good agreement with available weak-beam transmission electron microscopy [4]. An earlier density-functional theory calculation employed the quasicontinuum DFT method, where a small first-principles cell containing the dislocation is embedded in the strain field produced by atoms interacting through an interatomic force law based on the embedded atom method (EAM) [5]. The disagreement between the QC-DFT-EAM calculation and both our calculation and the experimental results most likely stems from the small (84 atom) cell used for the first-principles calculations. Our reference calculations indicate that these cell dimensions are too small to isolate the dislocation core elastically or electrostatically from the surface of the metal cluster. Peierls-Nabarro models [6,7] are not well suited for describing details of the strain field in the partial core as it is represented only indirectly through the generalized stacking fault energy. Different implementations of the Peierls-Nabarro model predict different separations, though both are based on first-principles evaluations of the generalized stacking fault energy. The results of Schoeck show good agreement with the measured separation distance between Shockley partials for an edge dislocation [7]. Several atomistic calculations for Al dislocations are based on central force potentials [11,31] and a new angular dependent potential [10]. Surprisingly, groups using the same atomistic poten-

TABLE II. Shockley partial splitting distances for $a/2\langle 110\rangle$ screw and edge dislocations. Experimental measurements for the edge dislocation are from weak-beam transmission electron microscopy (WB-TEM) [4]. FP-GFBC is the current work showing two measurements of the separation (cf. Figs. 1 and 2). The quasicontinuum calculation (QC-DFT-EAM), the Peierls-Nabarro methods, and the embedded atom methods (EAM, EAM2, BAM) are described briefly in the text.

Method	Screw [Å]	Edge [Å]
	Experiment	
WB-TEM [4]		8.0
	Density-functional theory	
FP-GFBC(this work)	7.5 (DD), 5.0 (Nye)	9.5 (DD), 7.0 (Nye)
QC-DFT-EAM [5]		5.6
	Peierls-Nabarro	
Semidiscrete [6]	2.1	3.5
Generalized [7]		7.8
	Atomistic	
EAM [8]	4.9	
EAM [9]	8.8	14.7
EAM [10]	16.0	16.0
EAM2 [11]	5.2–5.5 (Nye)	5.4–6.2 (Nye)
BAM [10]		5.0/15.0

tial [31] have reported dramatically different results for the separation distance of the screw dislocation, ranging from 4.9 to 16 Å [8–10]; this variation is possible the result of different treatments for the boundary conditions. More recently developed EAM potentials for Al from Mishin *et al.* produce smaller separation distances than previous EAM potentials, in better agreement with the current work [11]. Finally, while elasticity theory suggests only one equilibrium configuration for Shockley partials spreading on the glide plane, Srinivasan *et al.*'s potential produced *two* stable partial separations at 5.0 and 15 Å. Such results are consistent with strong short-range angular bonding terms in the atomistic potential. This broad range in the predicted partial separation illustrates the sensitivity of the calculation to both the treatment of the local atomic interactions and the long-range boundary conditions. This reinforces the need for a self-consistent predictive method for modeling dislocation core structure.

Conclusion.—We have predicted the strain fields of isolated Al edge and screw dislocation using density-functional theory combined with a flexible boundary condition method. The calculated Shockley partial splitting distance for the edge dislocation is in good agreement with available experimental data. These predictions significantly narrow the range of splitting distances for both screw and edge dislocations thereby eliminating confusion stemming from the wide range of Al values in the literature. The accurate prediction of the atomic-scale core geometries for Al screw- and edge-character dislocations is needed to inform higher-length scale models of plasticity in Al alloys, as well as other fcc metals. Nowhere is this more important than in models of diffusion processes in Al alloys (e.g., Al-Mg) where thermodynamic inputs must be obtained from accurate solute or dislocation energetics. The wide range of dislocation geometries produced by atomistic simulations implies that such methods cannot provide accurate solute-dislocation interaction energies. FP-GFBC optimized screw and core structures can now serve as the basis for computing quantities such as the Al core activation enthalpy for diffusion and solute-dislocation energetics for such important alloying agents as Mg, Cu, Mn, Li, Zn, and Si, and provide a basis for understanding the influence of trace elements such as Fe. While these calculations are challenging, precise predictions of the dislocation core geometry from electronic structure calculations is now possible with current tools and computational resources.

The authors thank W. Curtin, D. Dimiduk, and Y. Mishin for helpful discussions. This research was performed with support from the Air Force Office of Scientific Research at the U.S. Air Force Research Laboratory (task No. 2306AL3P), the MURI program "Virtual Design and Testing of Materials: A Multiscale Approach" at Brown University, and while D. R. T. held an NRC Research Associate grant at AFRL. L. G. H. and D. L. O. acknowledge the support of the General Motors/Brown Collaborative Research Lab on Computational Materials Science. This research was supported in part by a grant of computer time from the DoD High Performance Computing Modernization Program at ASC/MSRC.

[1] J. P. Hirth and J. Lothe, *Theory of Dislocations* (John Wiley & Sons, New York, 1982), 2nd ed.
[2] M. J. Mills, M. S. Daw, and S. M. Foiles, Ultramicroscopy **56**, 79 (1994).
[3] C. Woodward, Mater. Sci. Eng. A **400–401**, 59 (2005).
[4] W. Höllerbauer and H. P. Karnthaler, Beitr. Elektronenmikroskop. Direktabb. Oberfl. **14**, 361 (1981).
[5] G. Lu, E. B. Tadmor, and E. Kaxiras, Phys. Rev. B **73**, 024108 (2006).
[6] G. Lu, N. Kioussis, V. V. Bulatov, and E. Kaxiras, Mater. Sci. Eng. A **309–310**, 142 (2001).
[7] G. Schoeck, Mater. Sci. Eng. A **333**, 390 (2002).
[8] V. V. Bulatov, O. Richmond, and M. V. Glazov, Acta Mater. **47**, 3507 (1999).
[9] D. L. Olmsted and R. D. Phillips (to be published).
[10] S. G. Srinivasan, X. Z. Liao, M. I. Baskes, R. J. McCabe, Y. H. Zhao, and Y. T. Zhu, Phys. Rev. Lett. **94**, 125502 (2005).
[11] Y. Mishin, D. Farkas, M. J. Mehl, and D. A. Papaconstantopoulus, Phys. Rev. B **59**, 3393 (1999).
[12] R. C. Picu, Acta Mater. **52**, 3447 (2004).
[13] W. A. Curtin, D. L. Olmsted, and L. G. Hector, Jr., Nat. Mater. **5**, 875 (2006).
[14] J. M. Robinson and M. P. Shaw, Int. Mater. Rev. **39**, 113 (1994).
[15] C. Woodward and S. Rao, Phys. Rev. Lett. **88**, 216402 (2002).
[16] M. J. Cawkwell, D. Nguyen-Manh, C. Woodward, D. G. Pettifor, and V. Vitek, Science **309**, 1059 (2005).
[17] C. Woodward and S. I. Rao, Philos. Mag. **84**, 401 (2004).
[18] G. Kresse and J. Hafner, Phys. Rev. B **47**, 558 (1993).
[19] G. Kresse and J. Furthmüller, Phys. Rev. B **54**, 11169 (1996).
[20] D. Vanderbilt, Phys. Rev. B **41**, 7892 (1990).
[21] G. Kresse and J. Hafner, J. Phys. Condens. Matter **6**, 8245 (1994).
[22] J. P. Perdew, in *Electronic Structure of Solids '91*, edited by P. Ziesche and H. Eschrig (Akademie Verlag, Berlin, 1991), pp. 11–20.
[23] W. B. Pearson, *A Handbook of Lattice Spacings and Structures of Metals and Alloys* (Pergamon Press, NY, 1967).
[24] G. Simmons and H. Wang, *Single Crystal Elastic Constants* (MIT Press, Cambridge, MA, 1971).
[25] R. H. Rautioaho, Phys. Status Solidi B **112**, 83 (1982).
[26] K. H. Westmacott and R. L. Peck, Philos. Mag. **23**, 611 (1971).
[27] A. F. Wright, M. S. Daw, and C. Y. Fong, Philos. Mag. A **66**, 387 (1992).
[28] P. J. H. Denteneer and J. M. Soler, J. Phys. Condens. Matter **3**, 8777 (1991).
[29] D. R. Trinkle, arXiv:cond-mat/0607388v1.
[30] C. S. Hartley and Y. Mishin, Acta Mater. **53**, 1313 (2005).
[31] F. Ercolessi and J. B. Adams, Europhys. Lett. **26**, 583 (1994).